International Journal of Engineering Sciences &Research Technology

(A Peer Reviewed Online Journal)
Impact Factor: 5.164

IJESRT

RESEARCHERID
THOMSON REUTERS

ISSN: 2277-9655
[Fang Li* *et al.*, 8(4): April, 2019] Impact Factor: 5.164
IC™ Value: 3.00 CODEN: IJESS7

IJESRT

INTERNATIONAL JOURNAL OF ENGINEERING SCIENCES & RESEARCH TECHNOLOGY

SYNTHESIS, STRUCTURE AND OPTICAL PROPERTIES OF ORGANIC INORGANIC HYBRID PEROVSKITES $(C_4H_9NH_3)_2PBBR_4$ AND $(C_6H_5CH_2NH_3)_2PBBR_4$

Shuai Liu, Fang Li *, Yahui Liu, Litu Xu, Fuqiang Yao & Xiaobo Han

* Hubei Key Laboratory of Optical Information and Pattern Recognition, Wuhan Institute of Technology, Wuhan 430205, PR China

DOI: 10.5281/zenodo.2650935

ABSTRACT

Organic inorganic hybrid perovskites have potential applications in solar cells, electroluminescent device, nanolaser and radiation detection because of their unique optoelectronic properties. In this paper,the perovskite $(C_4H_9NH_3)_2PbBr_4$ and $(C_6H_5CH_2NH_3)_2PbBr_4$ were synthesized by solvent evaporation. The crystal structure, morphology, absorption spectrum, laser power dependence ofthe PL intensity and lifetime were studied. The results show that both two perovskitesare well crystallized and oriented. The absorption peaks are located at 416 nm (2.96 eV) and 392 nm (3.16 eV), the PL peaks are located at 427 nm (2.81 eV) and 415 nm (298 eV) respectively. The PL intensity increases with increasing laser power, but the lifetime decreases with increasing laser power, which is mainly due to the non-geminate recombination.

KEYWORDS: organic inorganic hybrid perovskites; two-photon photoluminescence; photoluminescence lifetime.

1. INTRODUCTION

Organic inorganic hybrid perovskites have received wide attention as the most competitive candidate in photovoltaic field recently [1-3]. The general chemical formula of the perovskite is ABX_3, in which A-sites are the organic ammonium cations, B-sites are the metal cations, X-sites are the halide anions. The B-site cations and X-sites anions form $[BX_6]$ octahedrons by ionic interaction, which are corner-sharing to constitute three-dimensional frameworks. The A-site cations are located in the frameworks cavity [4-6]. The two-dimensional layered perovskites consist of the inorganic octahedrons frameworks sandwiched between the bilayers of organic component. The excitons in the inorganic layer display special optical properties such as nonlinear absorption [7] and excitonic emission [8]. The strong exciton peaks in the optical spectra are attributed to the large exciton binding energy at room temperature [9]. Organic inorganic hybrid perovskites have great potential applications in solar cells [10-12], electroluminescent devices [13,14], nanolaser [15-17] and photodetections[18,19].

The conventional photovoltaic requires expensive materials and complex fabrication procedures. Organic inorganic hybrid perovskites as light harvesters of solar cells has revolutionized the prospects of photovoltaic technology. In 2009, Miyasaka et al. [20] initially studied the solar cells with the perovskite$CH_3NH_3PbI_3$, yielding a power conversion efficiency (PCE) of only 3.8%. In 2012, Kawano et al. [21] studied the optical properties of the perovskites $(C_{10}H_7CH_2NH_3)_2PbBr_xI_{4-x}$, they found that the near-resonant transition energies between Wannier and Frenkel excitons increases with an enhancement of iodine. In 2015, Slavney et al. [22] synthesized double perovskite structure compound $Cs_2AgBiBr_6$. It was significantly more heat and moisture stable compared to the perovskite$CH_3NH_3PbI_3$ and displayed long carrier recombination lifetime. In 2017, Hu et al. [23] studied the perovskite$CsPbBr_3$nanoplateelectroluminescence devices, which displayed a narrow EL peak centered at 530 nm with a narrow full width at half-maximum of 22 nm. In 2017, Chen et al. [24] prepare the perovskite $(C_4H_9NH_3)_2PbBr_4$ by ternary solvent method and studied the effect of the crystallization temperature, solvent volume ratio on the morphology. In 2018, Luo et al. [25] studied the solar cells with the inverted planar

ISSN: 2277-9655
Impact Factor: 5.164
CODEN: IJESS7

heterojunction perovskite, yielding a PCE of 21% due to the elimination of nonradiative charge-carrier recombination.

The different properties of organic and inorganic components are united in an independent composite. The inorganic component provides the opportunities for high carrier mobility and a wide range of bandgap. The organic component offers the possibility of structural diversity and high photoluminescence quantum yield. Moreover these properties can be easily modified by changing the organic ammonium, metal or halide [26]. In this paper, the perovskite $(C_4H_9NH_3)_2PbBr_4$ and $(C_6H_5CH_2NH_3)_2PbBr_4$ are synthesized by solvent evaporation. The laser power effect on the PL intensity and lifetime was investigated with femtosecond laser via the two-photon excitation.

2. MATERIALS AND METHODS

2.1. Synthesis of organic ammonium salts

Equally volume of HBr was added in the $C_4H_9NH_2$ and $C_6H_5CH_2NH_2$ respectively. The mixtures were heated at 50℃ and then cooled at room temperature. The organic ammonium salts $C_4H_9NH_3Br$ and $C_6H_5CH_2NH_3Br$ were obtained.

2.2. Synthesis of perovskite crystals

The stoichiometric quantities of organic ammonium salts and $PbBr_2$ were dissolved in N,N-dimethylformamide (DMF) respectively. The mixtures were heated at 50℃ and stirred for 1 hour, the perovskite $(C_4H_9NH_3)_2PbBr_4$ and $(C_6H_5CH_2NH_3)_2PbBr_4$were prepared by solvent evaporation. The products were washed with ethanol followed by heat treatment.

2.3. Synthesis of perovskite nanosheets

The perovskite crystals were ground into powders, which were used for XRD measurement. The perovskite powders were put in aqueous solution, ultrasonically processed, and then centrifuged. After a period of time, large quantities of perovskite nanosheets were obtained for TEM measurement. The chemical reaction equations involved in the experiment are as follows:

$$C_4H_9NH_2 + HBr \Rightarrow C_4H_9NH_3Br \quad (1)$$

$$2C_4H_9NH_3Br + PbBr_2 \Rightarrow (C_4H_9NH_3)_2PbBr_4 \quad (2)$$

$$C_6H_5CH_2NH_2 + HBr \Rightarrow C_6H_5CH_2NH_3Br \quad (3)$$

$$2C_6H_5CH_2NH_3Br + PbBr_2 \Rightarrow (C_6H_5CH_2NH_3)_2PbBr_4 \quad (4)$$

2.4. Characterization

The structure was analyzed by X-ray diffraction (Germany Bruker AXS, D8 Advance). The morphology was observed by transmission electron microscopy (Japan JEOL, JEM-2000). The absorption spectra was measured with UV-visible spectrometer (America PerkinElmer, Lambda 35). The optical measurements were performed using a commercial optical microscope system (Japan, Olympus IX73). A Ti:sapphire oscillator (China Atop Electronic Technology Co. Ltd., Vitara) was used for two-photon excitation. The laser beam was focused by an objective (Olympus, NA = 0.65) onto the samples. The reflected signal was collected by the same objective and then directed into a spectrometer (Andor 193i) for spectral measurement or onto a CCD camera for imaging. The time correlated single photon count (TCSPC) system consisting of a PicoHarp 300 controller, a PDL 800-B reference and a SPDA-15 detector is used for the lifetime measurements. The experimental results can be fitted to a biexponential decay function:

$$I = A_1 \exp(-t/\tau_1) + A_2 \exp(-t/\tau_2) \quad (5)$$

τ_1 and τ_2 are the radiative and nonradiative decay lifetime respectively. Figure 1 shows the optical path of the photoluminescence test system used in the experiment, in which A1 and A2 are half wave plates; B is polarizer;

ISSN: 2277-9655
Impact Factor: 5.164
CODEN: IJESS7

C1 and C2 are low pass filters; M1～M7 and M9～M11 are reflectors; M8 is reflex; O1 and O2 are objectives; CCD is charge couple device.

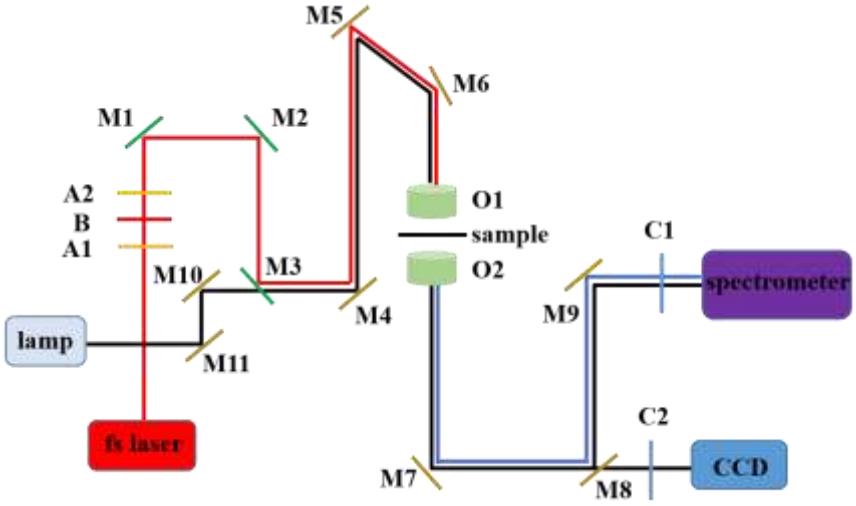

Figure 1. The experiment optical path of photoluminescence test system

3. RESULTS AND DISCUSSION

3.1. Structure characterization

Figure 2(a) and 2(b) show the crystal structure of the perovskite $(C_4H_9NH_3)_2PbBr_4$ and $(C_6H_5CH_2NH_3)_2PbBr_4$. It can be observed the two perovskites exhibit the two dimensional layered structures with alternating organic and inorganic components. The Pb cations and Br anions form $[PbBr_6]$ octahedrons by ionic interaction, which are corner-sharing to constitute the frameworks. The organic ammonium cations are located in the cavity of the $[PbBr_6]$ octahedrons. The growth directions of the perovskite layers are along the c axis and a axis, respectively. The lattice parameters of the perovskite $(C_4H_9NH_3)_2PbBr_4$ and $(C_6H_5CH_2NH_3)_2PbBr_4$ are a=0.822 nm, b=0.833 nm, c=2.762 nm and a=3.3394 nm, b=0.8153 nm, c=0.8131 nm, which are consistent with reports in the literature [27,28].

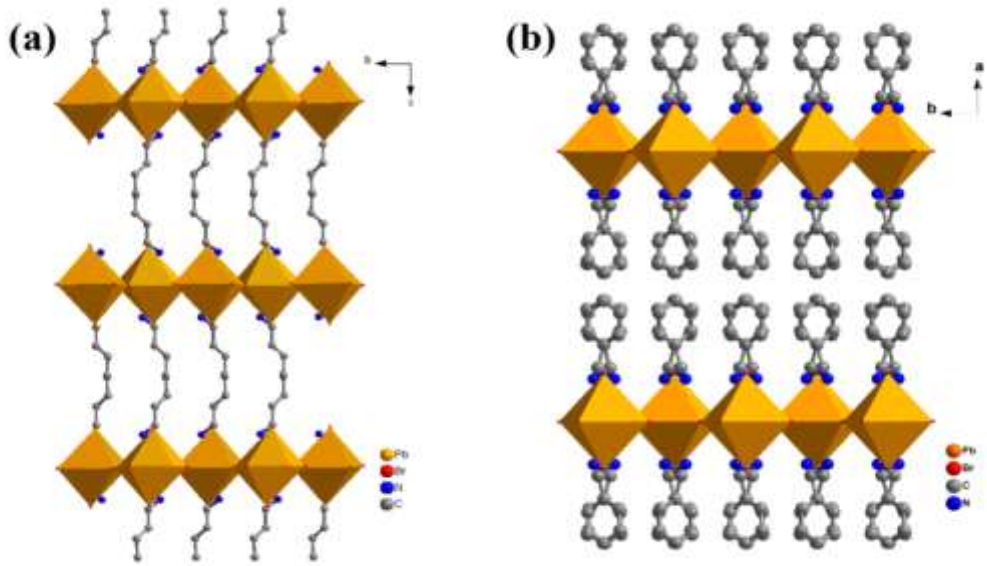

Figure 2. The crystal structure of the perovskite (a) $(C_4H_9NH_3)_2PbBr_4$; (b) $(C_6H_5CH_2NH_3)_2PbBr_4$. The hydrogen atoms bonded to the carbon atoms are omitted for clarity.

ISSN: 2277-9655
Impact Factor: 5.164
CODEN: IJESS7

Figure 3(a) and 3(b) show the XRD patterns of the perovskite powders $(C_4H_9NH_3)_2PbBr_4$ and $(C_6H_5CH_2NH_3)_2PbBr_4$. The diffraction peaks of the perovskite $(C_4H_9NH_3)_2PbBr_4$ are located at 6.42°, 12.85°, 19.33°, 25.87° and 32.5°, which are corresponding to the lattice plane (00X, X=2, 4, 6, 8, …). The diffraction peaks of the perovskite $(C_6H_5CH_2NH_3)_2PbBr_4$ are located at 6.41°, 10.63°, 15.96°, 21.32°, 26.72°, 32.18° and 37.73°, which are corresponding to the lattice plane (X00, X=2, 4, 6, 8, …). All the patterns confirm that the two perovskites are well crystallized and oriented. The interlayer spacing of the perovskites are calculated using the Bragg formula:

$$2d\sin\theta = k\lambda \tag{6}$$

d is the interlayer spacing, θ is the diffraction degree, k is the diffraction class, λ is the wavelength of X-ray. The interlayer spacing of the two perovskites are 1.42 nm and 1.44 nm respectively according to the formula above.

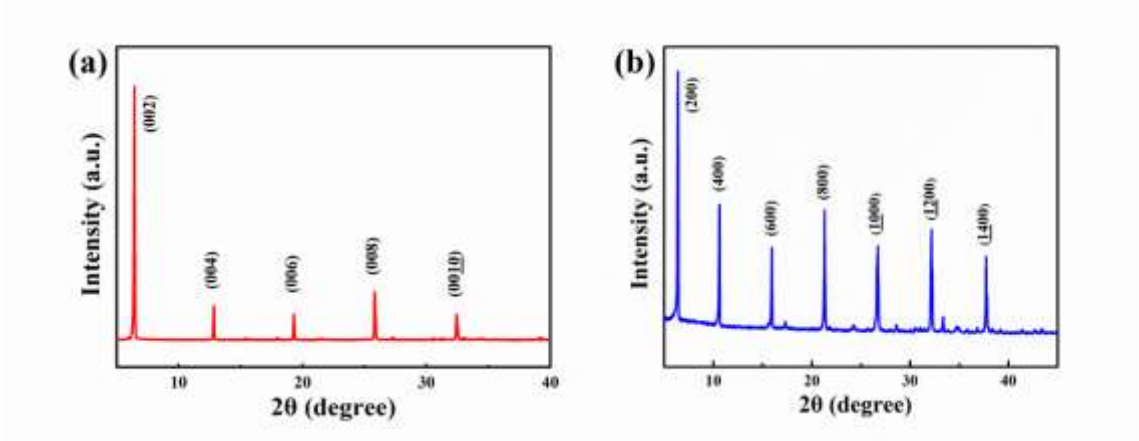

Figure 3. The XRD patterns of the perovskite powders (a) $(C_4H_9NH_3)_2PbBr_4$; (b) $(C_6H_5CH_2NH_3)_2PbBr_4$

3.2. Morphology characterization

Figure 4(a) shows the bright field TEM images of the perovskite $(C_4H_9NH_3)_2PbBr_4$nanosheets. The perovskite $(C_4H_9NH_3)_2PbBr_4$ displays a layered stacking structure with crystal geometry size of 1.6 um. Figure 4(b) shows the HR-TEM images of the perovskite $(C_6H_5CH_2NH_3)_2PbBr_4$nanosheets. It shows that the lattice plane has the spacing distance of 0.277 nm, with the growth direction along [001]. The selected area electron diffraction (SAED) pattern of the perovskite $(C_4H_9NH_3)_2PbBr_4$nanosheets is shown in Figure 4(c), indicating the orthorhombic phase, space group Pbca, with a growth direction along [001]. Figure 4(d) shows the bright field TEM images of the perovskite $(C_6H_5CH_2NH_3)_2PbBr_4$nanosheets. The perovskite $(C_6H_5CH_2NH_3)_2PbBr_4$ displays a layered stacking structure with crystal geometry size of 800 nm. Figure 4(e) shows the HR-TEM images of the perovskite $(C_6H_5CH_2NH_3)_2PbBr_4$nanosheets. It shows that the lattice plane has the spacing distance of 0.294 nm, with the growth direction along [100]. The selected area electron diffraction (SAED) pattern of the perovskite $(C_6H_5CH_2NH_3)_2PbBr_4$nanosheets is shown in Figure 4(f), indicating the orthorhombic phase, space group Cmca, with a growth direction along [100].

ISSN: 2277-9655
Impact Factor: 5.164
CODEN: IJESS7

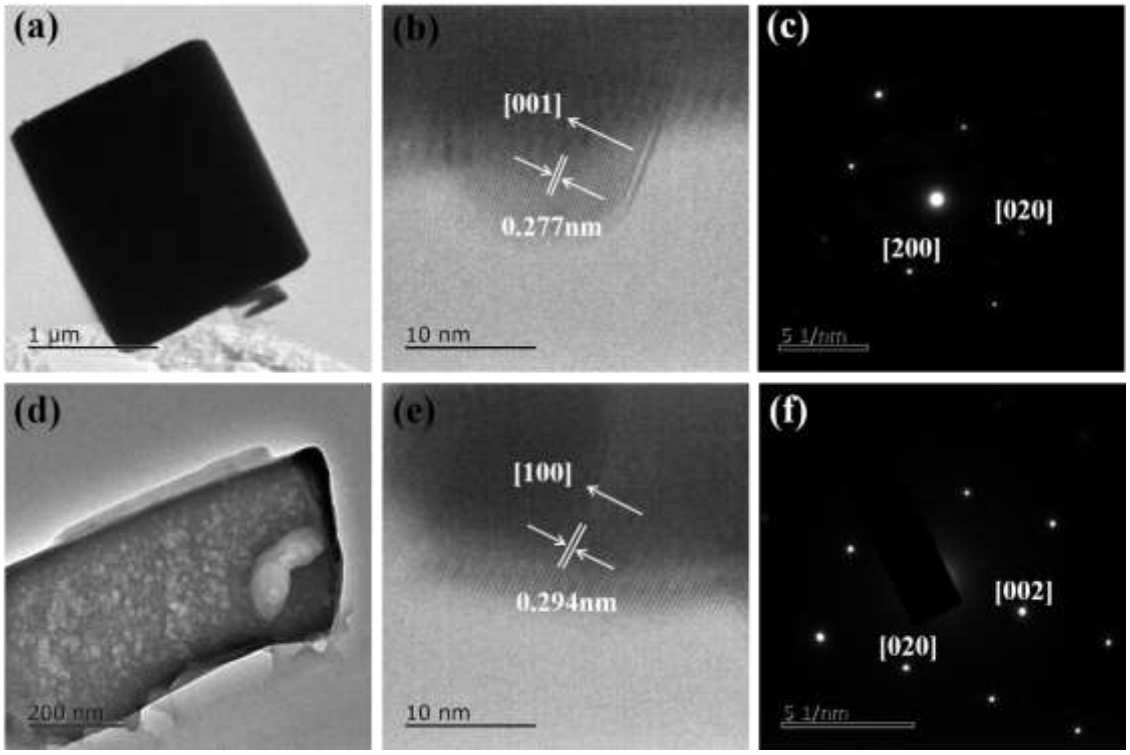

Figure 4. (a) The bright field TEM images, (b) HR-TEM images and (c) SAED pattern of the perovskite $(C_4H_9NH_3)_2PbBr_4$nanosheets; (d) the bright field TEM images, (e) HR-TEM images and (f) SAED pattern of the perovskite $(C_6H_5CH_2NH_3)_2PbBr_4$nanosheets.

3.3. Absorption spectrum

Figure 5 shows the absorption spectrum of the perovskites $(C_4H_9NH_3)_2PbBr_4$ (red curve) and $(C_6H_5CH_2NH_3)_2PbBr_4$ (blue curve).The absorption peaks are located at 416 nm (2.96eV) and 392 nm (3.16eV), which belong to the typical excitonic absorption peaks. Organic inorganic hybrid perovskites have multiple quantum well structures with alternating organic and inorganic layer, therefore the excitons possess larger binding energy and exhibit strong exciton absorption due to quantum confinement effect.

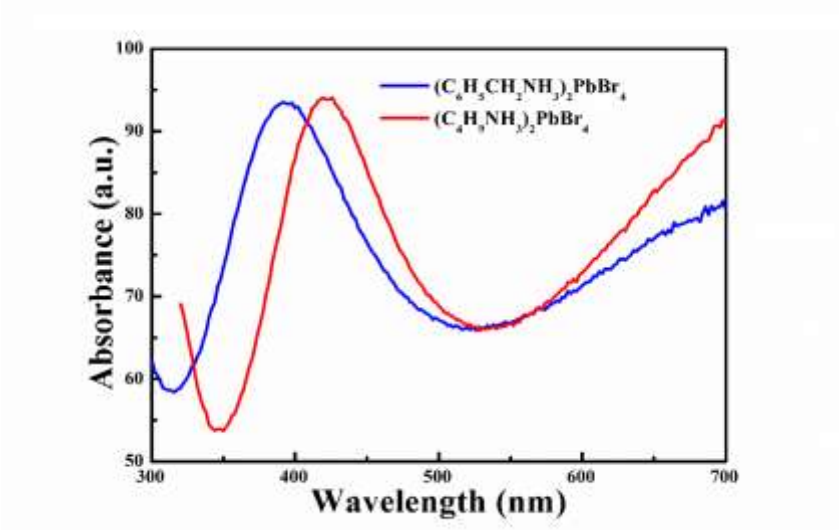

Figure 5. The absorption spectrum of the perovskite $(C_4H_9NH_3)_2PbBr_4$ (red curve) and $(C_6H_5CH_2NH_3)_2PbBr_4$ (blue curve).

ISSN: 2277-9655
Impact Factor: 5.164
CODEN: IJESS7

3.4. The laser power effect on the PL intensity

Figure 6(a) and 6(b) show the bright field and dark field optical microscope images of the perovskites $(C_4H_9NH_3)_2PbBr_4$ and $(C_6H_5CH_2NH_3)_2PbBr_4$. It is possible to observe the regular and transparent crystal geometry of the two perovskites, which emit blue photoluminescence under the femtosecond laser. Figure 6(c) and 6(d) show the two-photon PL spectrum of the perovskites $(C_4H_9NH_3)_2PbBr_4$ and $(C_6H_5CH_2NH_3)_2PbBr_4$. PL peaks are located at 427 nm (2.81 eV) and 415 nm (298 eV) respectively [28,29]. When the laser power is set to 40, 60, 70, 80 and 90mW, the PL intensity of the perovskite $(C_4H_9NH_3)_2PbBr_4$ are 2320, 5227, 8216, 10390 and 13224 photon counts; while the PL intensity of the perovskite $(C_6H_5CH_2NH_3)_2PbBr_4$ are 733, 1233, 1407, 1857 and 2195 photon counts. Both the two perovskites display an increasing trend with the enhancement of the laser power. Moreover the PL intensity of the perovskite $(C_4H_9NH_3)_2PbBr_4$ is higher than $(C_6H_5CH_2NH_3)_2PbBr_4$ at the same laser power. The interlayer spacing of the perovskite $(C_6H_5CH_2NH_3)_2PbBr_4$ is larger than $(C_4H_9NH_3)_2PbBr_4$. The increase of interlayer spacing leads to the reduction of inorganic layer thickness, which causing the enhancement of exciton binding energy. Therefore the exciton of the perovskite $(C_4H_9NH_3)_2PbBr_4$ is easier to separate, transfer and recombination.

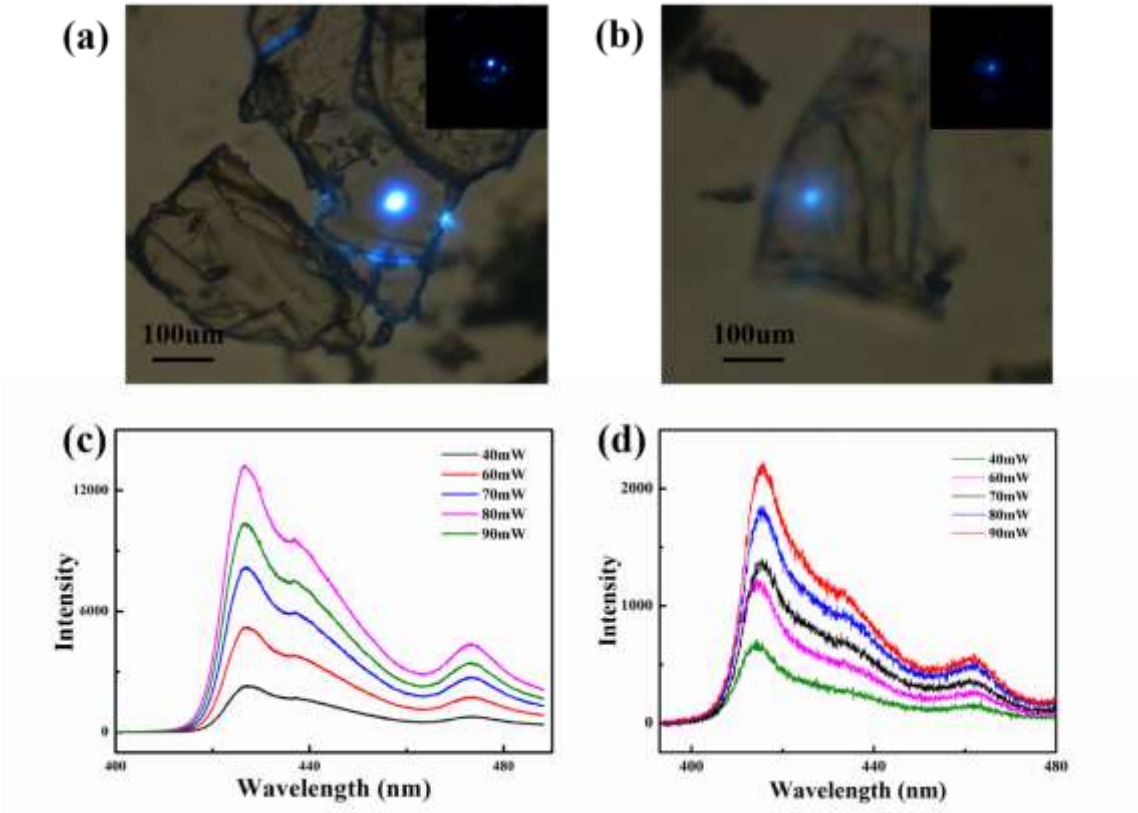

Figure 6. The optical microscope images of the perovskite (a) $(C_4H_9NH_3)_2PbBr_4$; (b) $(C_6H_5CH_2NH_3)_2PbBr_4$; the two-photon PL spectrum of the perovskite (c) $(C_4H_9NH_3)_2PbBr_4$; (d) $(C_6H_5CH_2NH_3)_2PbBr_4$.

3.5. The laser power effect on the PL lifetime

Figure 7(a) and 7(b) show the lifetime of the two-photon PL emission (pumped at 800 nm) from the perovskite $(C_4H_9NH_3)_2PbBr_4$ and $(C_6H_5CH_2NH_3)_2PbBr_4$. When the laser power is set to 40, 60, 70, 80 and 90mW, the perovskite $(C_4H_9NH_3)_2PbBr_4$ exhibits the decay lifetime of 3.02, 2.84, 2.62, 2.51 and 2.29 ns; while the perovskite $(C_6H_5CH_2NH_3)_2PbBr_4$ exhibits the decay lifetime of 3.02, 2.84, 2.62, 2.51 and 2.29 ns. Both the two perovskites display a decreasing trend with the enhancement of the laser power. Moreover the PL lifetime of the perovskite $(C_4H_9NH_3)_2PbBr_4$ is longer than $(C_6H_5CH_2NH_3)_2PbBr_4$ at the same laser power. The absorption and emission of photon originate from electron transition of inorganic layer rather than organic layer. The interlayer spacing of the perovskite $(C_6H_5CH_2NH_3)_2PbBr_4$ is larger than $(C_4H_9NH_3)_2PbBr_4$. The increase of

ISSN: 2277-9655
Impact Factor: 5.164
CODEN: IJESS7

interlayer spacing leads to the reduction of inorganic layer thickness, which causing the enhancement of exciton binding energy. Therefore the exciton of the perovskite $(C_4H_9NH_3)_2PbBr_4$ is easier to separate, transfer and recombination.

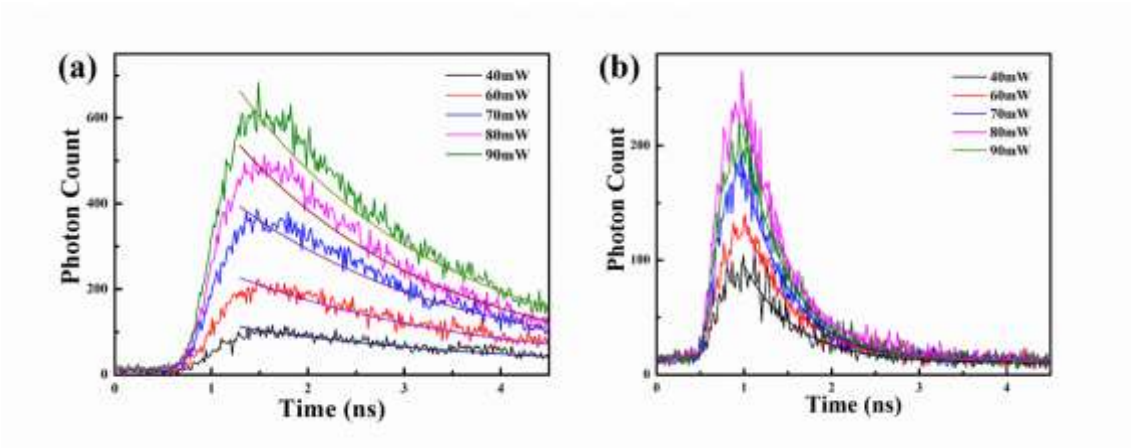

Figure 7. The PL decay profile of the perovskite (a) $(C_4H_9NH_3)_2PbBr_4$; (b) $(C_6H_5CH_2NH_3)_2PbBr_4$.

The fluence-dependence of PL intensity and lifetime with laser power can be explained with the energy level diagram [30-33], which is shown in Figure8. The perovskite molecules will absorb two photons after the 800 nm laser excitation, promoting the electron transfer from S_0 to S_1. Some electrons in S_1 will return to S_0, causing the excitonic emission process. Some other electrons in S_1will transfer to ESS through relaxation process. The relaxation to ESS, or ESS recombination can possess certain non-geminate recombination characteristics. This emission is a kind of non-geminate recombination, which is the intensity-dependent two-photon absorption cross-section [34,35]. When laser power increases, more electrons transfer from S_1 to S_0 and S_1 to ESS. As a consequence, the carrier density increases and the emission is dominated by non-geminate recombination, which results in the increase of PL intensity and decrease of lifetime.

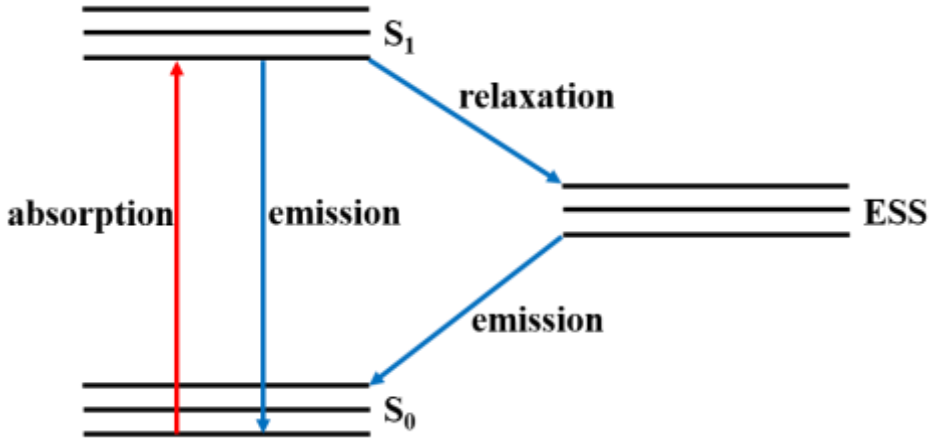

Figure 8. Energy level schemes of the organic inorganic hybrid perovskite. S_0, ground state; S_1, first excited singlet state; ESS, electron surface states.

4. CONCLUSION

In this paper, the perovskite $(C_4H_9NH_3)_2PbBr_4$ and $(C_6H_5CH_2NH_3)_2PbBr_4$ were synthesized by solvent evaporation. The crystal structure, morphology, absorption spectrum, laser power dependence of the PL intensity and lifetime were studied. The results show that the two perovskites are well crystallized and oriented. The absorption peaks are located at 416 nm (2.96 eV) and 392 nm (3.16 eV), the PL peaks are located at 427 nm (2.81 eV) and 415 nm (298 eV) respectively. The PL intensity increases with increasing laser power, but the lifetime decreases with increasing laser power, which is mainly due to the non-geminate recombination. The

ISSN: 2277-9655
Impact Factor: 5.164
CODEN: IJESS7

photoluminescence properties of organic inorganic hybrid perovskites can be modified during a wide range, which display potential applications in optoelectronic field.

5. ACKNOWLEDGEMENTS

This research was supported by the National Natural Science Foundation of China (Grant No. 11204222), the Natural Science Foundation of Hubei Province, China (Grant No. 2013CFB316, Grant No. 2014CFB793), the Innovation Fund of School of Science, Wuhan Institute of Technology (No. CX2016106).

REFERENCES

[1] B. Saparov, D.B. Mitzi, Organic Inorganic Perovskites: Structural Versatility for Functional Materials Design. Chem. Rev. 2016, 116, 4558-4596.
[2] W. Li, Z.M. Wang, F. Deschler, S. Gao, R.H. Friend, A.K. Cheetham, Chemically diverse and multifunctional hybrid, organic–inorganic perovskites. Nat. Rev. Mater. 2017, 2, 16099.
[3] E.Z. Shi, Y. Gao, B.P. Finkenauer, Akriti, A.H. Coffey, L. Dou, Two-dimensional halide perovskite nanomaterials and heterostructures. Chem. Soc. Rev. 2018.
[4] Y.X. Tian, A. Merdasa, E. Unger, M. Abdellah, K.B. Zheng, S. McKibbin, A. Mikkelsen, T. Pullerits, A. Yartsev, V. Sundstrom, I.G. Scheblykin, Enhanced Organo-Metal Halide Perovskite Photoluminescence from Nanosized Defect-Free Crystallites and Emitting Sites. J. Phys. Chem. Lett. 2015, 6, 4171-4177.
[5] T.W. Kim, S. Uchida, T. Matsushita, L. Cojocaru, R. Jono, K. Kimura, D. Matsubara, M. Shirai, K. Ito, H. Matsumoto, Self-Organized Superlattice and Phase Coexistence inside Thin Film Organometal Halide Perovskite. Adv. Mater. 2018, 30, 1705230.
[6] L.Y. Dong, S.J. Sun, Z.Y. Deng, W. Li, F.X. Wei, Y.J. Qi, Y.C. Li, X.D. Li, P.X. Lu, U.Ramamurty, Elastic properties and thermal expansion of lead-free halide double perovskite $Cs_2AgBiBr_6$.Comput. Mater. Sci. 2018, *141*, 49–58.
[7] X.B. Han, K. Wang, H. Long, H.B. Hu, J.W. Chen, B. Wang, P.X. Lu, Highly sensitive detection of the lattice distortion in single bent ZnO nanowires by second harmonic generation microscopy. ACS Photonics 2016, 3, 1308-1314.
[8] S.J. Zhang, P. Audebert, Y. Wei, A.A. Choueiry, G. Lanty, A. Bréhier, L. Galmiche, G. Clavier, C. Boissière, J.S. Lauret, E. Deleporte, Preparations and Characterizations of Luminescent Two Dimensional Organic-inorganic Perovskite Semiconductors. Materials 2010, 3, 3385-3406.
[9] N. Kawano, M. Koshimizu, Y. Sun, N. Yahaha, Y. Fujimoto, T. Yanagida, K. Asai, Effects of Organic Moieties on Luminescence Properties of Organic–Inorganic Layered Perovskite-Type Compounds. J. Phys. Chem. C. 2014, 118, 9101-9106.
[10] P.L. Qin, H.W. Lei, X.L. Zheng, Q. Liu, H. Tao, G. Yang, W.J. Ke, L.B. Xiong, M.C. Qin, X.Z. Zhao, G.J. Fang, Copper-Doped Chromium Oxide Hole-Transporting Layer for Perovskite Solar Cells: Interface Engineering and Performance Improvement. Adv. Mater. Interf. 2016, 3, 1500799.
[11] Q.R. Deng, Y.Q. Li, L.A. Chen, S.G. Wang, G.M. Wang, Y.L. Sheng, G.S. Shao, The effects of electron and hole transport layer with the electrode work function on perovskite solar cells. Mod. Phys. Lett. B 2016, 30, 1650341.
[12] P.L. Qin, Q. He, O.Y. Dan, G.J. Fang, W. Choy, G. Li, Transition metal oxides as hole-transporting materials in organic semiconductor and hybrid perovskite based solar cells. Sci. China Chem. **2017**, 60, 472-489.
[13] X. Qin, H.L. Dong, W.P. Hu, Green light-emitting diode from bromine based organic inorganic halide perovskite. Sci. China Mater. 2015, 58, 186-191.
[14] Z.K. Tan, R.S. Moghaddam, M.L. Lai, P. Docampo, R. Higler, F. Deschler, M. Price, A. Sadhanala, L.M. Pazos, D. Credgington, F. Hanusch, T. Bein, H.J. Snaith, R.H. Friend, Bright light emitting diodes based on organometal halide perovskite. Nat. Nanotechnol. 2014, 9, 687-692.
[15] L.T. Xu, F. Li, L. Wei, J.X. Zhou, S. Liu, Design of Surface Plasmon Nanolaser Based on MoS_2.Appl. Sci. 2018, *8*, 2110.
[16] L.T. Xu, F. Li, S. Liu, F.Q. Yao, Y.H. Liu, Low Threshold Plasmonic Nanolaser Based on Graphene. Appl. Sci. 2018, *8*, 2186.
[17] L.T. Xu, F. Li, Y.H. Liu, F.Q. Yao, S. Liu, Surface Plasmon Nanolaser: Principle, Structure,

ISSN: 2277-9655
Impact Factor: 5.164
CODEN: IJESS7

Characteristics and Applications. Appl. Sci. 2019, 9, 861.
[18] C.C. Stoumpos, C.D. Malliakas, J.A. Peters, Z.F. Liu, M. Sebastian, J. Im, T.C. Chasapis, A.C. Wibowo, D.Y. Chung, A.J. Freeman, B.W. Wessels, M.G. Kanatzidis, Crystal Growth of the Perovskite Semiconductor $CsPbBr_3$: A New Material for High-Energy Radiation Detection. Cryst. Growth Des. 2013, 13, 2722-2727.
[19] L.T. Dou, Y.M. Yang, J.B. You, Z.R. Hong, W.H. Chang, G. Li, Y. Yang, Solution processed hybrid perovskite photodetectors with high detectivity. Nat. Commun. 2014, 5, 5404.
[20] A. Kojima, K. Teshima, Y. Shirai. T. Miyasaka, Organometal halide perovskites as visible light sensitizers for photovoltaic cells. J. Am. Chem. Soc. 2009, 131, 6050-6051.
[21] N. Kawano, M. Koshimizu, K. Asai, The Effect of Wannier and Frenkel Exciton Resonance on the Luminescence Properties of Organic Inorganic Layered Perovskite-Type Compounds. J. Phys. Chem. C. 2012, 116, 22992–22995.
[22] A.H. Slavney, T. Hu, A.M. Lindenberg, H.I. Karunadasa, A Bismuth-Halide Double Perovskite with Long Carrier Recombination Lifetime for Photovoltaic Applications. J. Am. Chem. Soc. 2016, 138, 2138-2141.
[23] X.L. Hu, H. Zhou, Z.Y. Jiang, X. Wang, S.P. Yuan, J.Y. Lan, Y.P. Fu, X.H. Zhang, W.H. Zheng, X.X. Wang, X.L. Zhu, L. Liao, G.Z. Xu, S. Jin, A.L. Pan, Direct Vapor Growth of Perovskite $CsPbBr_3$ Nanoplate Electroluminescence Devices. ACS Nano. 2017, 11, 9869-9876.
[24] J.N. Chen, L. Gan, F.W. Zhuge, H.Q. Li, J.Z. Song, H.B. Zeng, T.Y. Zhai, A Ternary Solvent Method for Large Sized Two Dimensional Perovskites. Angew. Chem. Int. Ed. 2017, 56, 2390-2394.
[25] D. Luo, W. Yang, Z. Wang, A. Sadhanala, Q. Hu, R. Su, Enhanced photovoltage for inverted planar heterojunction perovskite solar cells. Science **2018,** 360, 1442-1446.
[26] C. Chen, Y.C. He, Z.P. Du, H. Yuan, Y.X. Wu, Preparation and properties of perovskite-type $La_{0.5}Pb_{0.5}MnO_3$ by stearic acid method. Mater. Lett. 2013, 110, 264-266.
[27] L.T. Dou, A.B. Wong, Y. Yu, M.L. Lai, N. Kornienko, S.W. Eaton, A. Fu, C.G. Bischak, J. Ma, T. Ding, N.S. Ginsberg, L.W. Wang, A.P. Alivisatos, P.D. Yang, Atomically thin two dimensional organic inorganic hybrid perovskites. Science 2015, 349, 1518-1521.
[28] W.Q. Liao, Y. Zhang, C.L. Hu, J.G. Mao, H.Y. Ye, P.F. Li, S.D. Huang, R.G. Xiong, A lead-halide perovskite molecular ferroelectric semiconductor. Nat. Commun. 2015, 6, 7338.
[29] Z.J. Tan, Y. Wu, H. Hong, J.B. Yin, J.C. Zhang, L. Lin, M.Z. Wang, X. Sun, L.Z. Sun, Y.C. Huang, K.H. Liu, Z.F. Liu, H.L. Peng, Two Dimensional $(C_4H_9NH_3)_2PbBr_4$Perovskite Crystals for High-Performance Photodetector. J. Am. Chem. Soc. 2016, 138, 16612-16615.
[30] F. Li, Z.C. He, M.Y. Li, J.P. Zhang, J.B. Han, P.X. Lu, Photoinduced energy transfer in a CdTe quantum dot–copper phthalocyanine system via two-photon excitation. Mater. Lett. 2014, *132*, 263–266.
[31] M.Y Li, F. Li, Z.C. He, J.P. Zhang, J.B. Han, P.X. Lu, Two-photon-excited fluorescence resonance energy transfer in an aqueous system of CdTe quantum dots and Rhodamine B. J. Appl. Phys. 2014, 116, 233106.
[32] F. Li, P.X. Lu, H. Long, G. Yang, Y.H. Li, Q.G. Zheng, Nonlinear absorption in PMMA-doped CuPc thin film in the femtosecond regime: Experimental and theoretical studies. Optics Express, 2008, 16, 14571-14581.
[33] F. Li, X.G. Li, Theoretical investigation on nonlinear absorption of multilevel organic molecular system in ns, ps and fs regime, Opt. Communications,2012, 285, 5217-5222.
[34] S. Liu, F. Li, X.B. Han, L.T. Xu, F.Q. Yao, Y.H. Liu, Preparation and Two Photon Photoluminescence Properties of Organic Inorganic Hybrid Perovskites $(C_6H_5CH_2NH_3)_2PbBr_4$ and $(C_6H_5CH_2NH_3)_2PbI_4$. Appl. Sci. 2018, 8, 2286.
[35] W.W. Liu, J. Xing, J.X. Zhao, X.L. Wen, K. Wang, P.X. Lu, Giant Two-Photon Absorption and Its Saturation in 2D Organic-Inorganic Perovskite. Adv. Opt. Mater. 2017, 5, 1601045.